Developmental Cell, Volume *37*

Supplemental Information

Centriolar CPAP/SAS-4 Imparts Slow Processive Microtubule Growth

Ashwani Sharma, Amol Aher, Nicola J. Dynes, Daniel Frey, Eugene A. Katrukha, Rolf Jaussi, Ilya Grigoriev, Marie Croisier, Richard A. Kammerer, Anna Akhmanova, Pierre Gönczy, and Michel O. Steinmetz

Figure S1

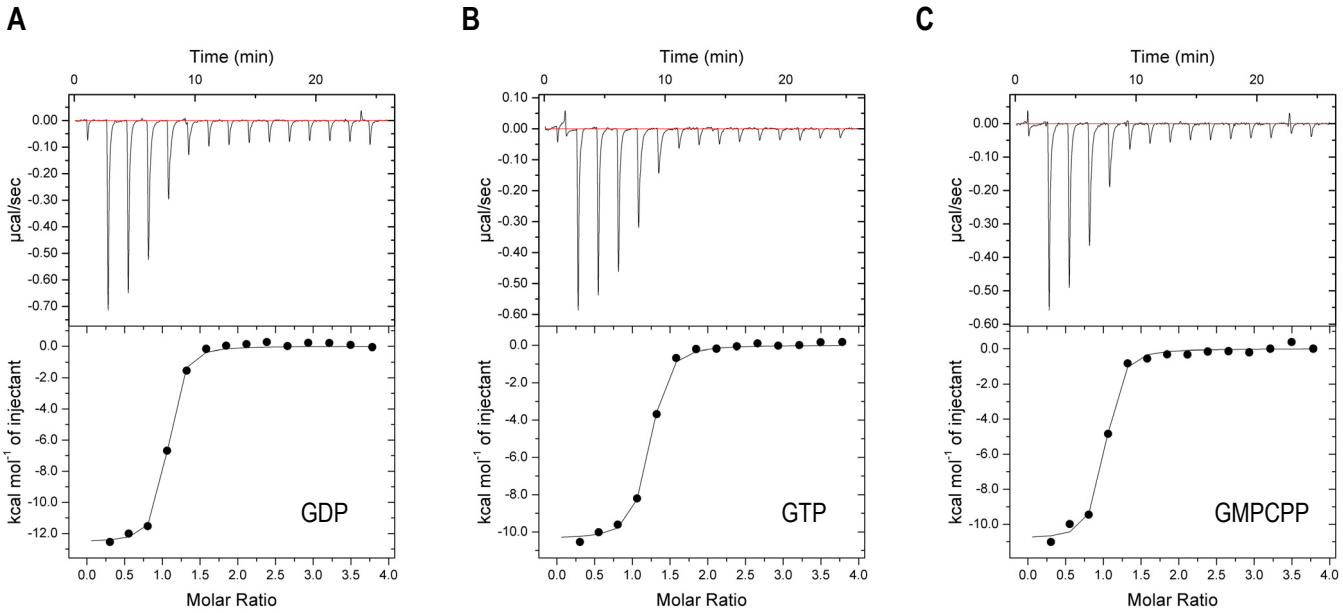
A
B
C
Time (min)
µcal/sec
kcal mol-1 of injectant
Molar Ratio
GDP
GTP
GMPCPP

Figure S1, related to Figure 2. Effect of nucleotide state of tubulin on the interaction with PN2-3s.

(A-C) ITC analysis of the interaction between PN2-3s and tubulin. Experiments were performed by step wise titration of 200 μM PN2-3s in the syringe into 10 μM tubulin in the cell. Upper panels display raw data; lower panels show the integrated heat changes and associated curve fits. The derived Kd values are as follows: 75 ± 12 nM for GDP-tubulin (A), 99 ± 13 nM for GTP-tubulin (B), and 97 ± 20 nM for GMPCPP-tubulin (C).

Figure S2

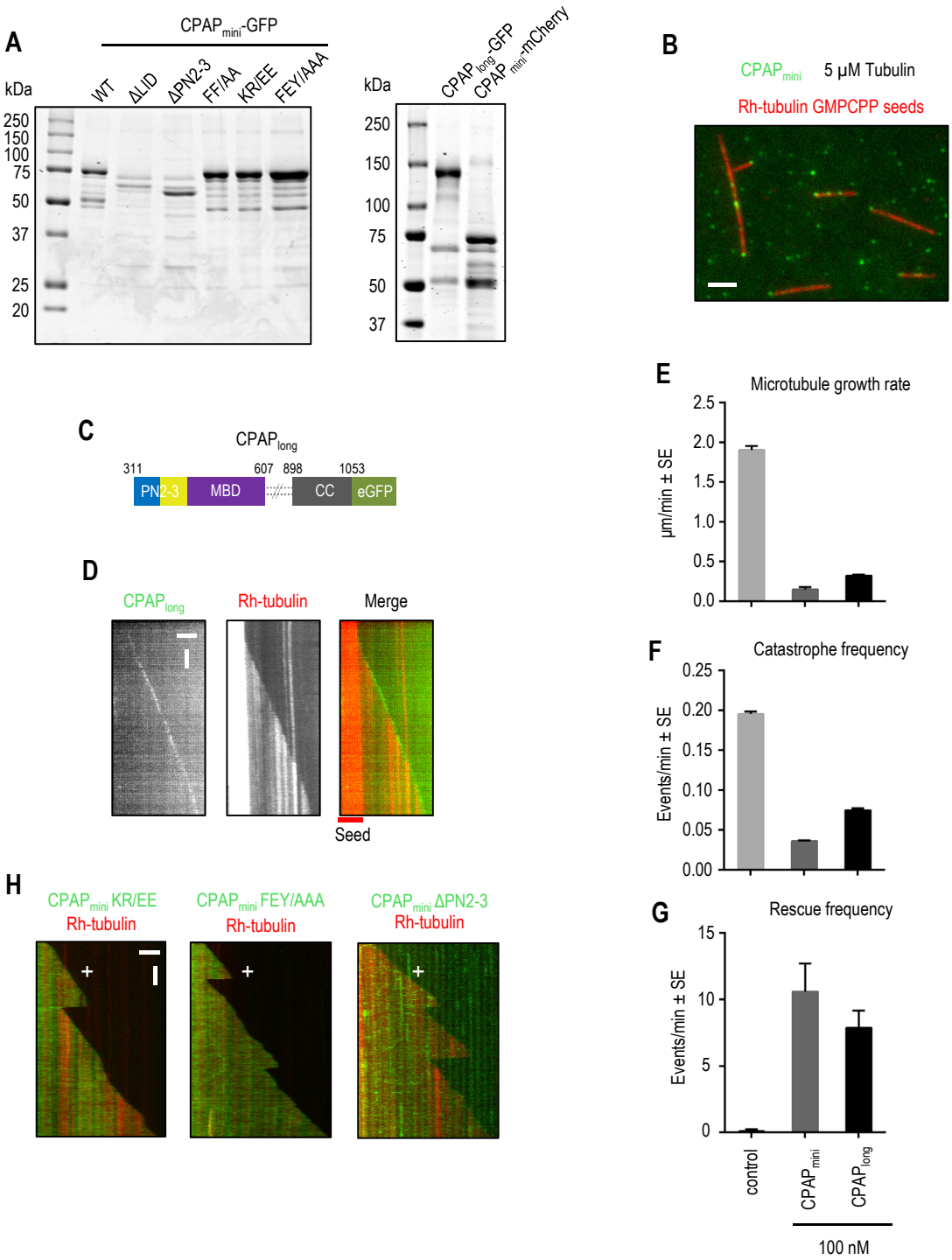
A
CPAP$_{mini}$-GFP
kDa
WT
ΔLID
ΔPN2-3
FF/AA
KR/EE
FEY/AAA
250
150
100
75
50
37
25
20
kDa
CPAP$_{long}$-GFP
CPAP$_{mini}$-mCherry
250
150
100
75
50
37
B
CPAP$_{mini}$ 5 µM Tubulin
Rh-tubulin GMPCPP seeds
C
CPAP$_{long}$
311
607
898
1053
PN2-3
MBD
CC
eGFP
D
CPAP$_{long}$
Rh-tubulin
Merge
Seed
E
Microtubule growth rate
µm/min ± SE
2.5
2.0
1.5
1.0
0.5
0.0
F
Catastrophe frequency
Events/min ± SE
0.25
0.20
0.15
0.10
0.05
0.00
G
Rescue frequency
Events/min ± SE
15
10
5
0
control
CPAP$_{mini}$
CPAP$_{long}$
100 nM
H
CPAP$_{mini}$ KR/EE
Rh-tubulin
CPAP$_{mini}$ FEY/AAA
Rh-tubulin
CPAP$_{mini}$ ΔPN2-3
Rh-tubulin
+
+
+

Figure S2, related to Figure 3. Characterization of the effect of $CPAP_{mini}$ on microtubule dynamics in vitro.

(A) Coomassie blue stained gel with $CPAP_{long}$, $CPAP_{mini}$ and its mutants purified from HEK293T cells.

(B) Localization of $CPAP_{mini}$ (green) on rhodamine-labelled GMPCPP stabilized microtubules (red) in the presence of 5 μM tubulin. Although no microtubule growth is observed in these conditions, $CPAP_{mini}$ preferentially binds to one microtubule end, indicating that its plus-end localization does not depend on microtubule polymerization.

(C) Schematic of the $CPAP_{long}$ construct.

(D) Kymograph of microtubule growth at the plus (+) end from a rhodamine-GMPCPP seed with 100 nM CPAPlong. Scale bars, 2 μm (horizontal) and 60 s (vertical).

(E-G) Microtubule plus-end growth rates, catastrophe and rescue frequencies in the presence of rhodamine-tubulin alone or together with CPAPmini-GFP or $CPAP_{long}$-GFP. Error bars represent SEM.

(H) Representative dual-color kymographs showing microtubule plus end dynamics for microtubules grown in the presence of rhodamine-tubulin together with the indicated $CPAP_{mini}$ variants.

Figure S3

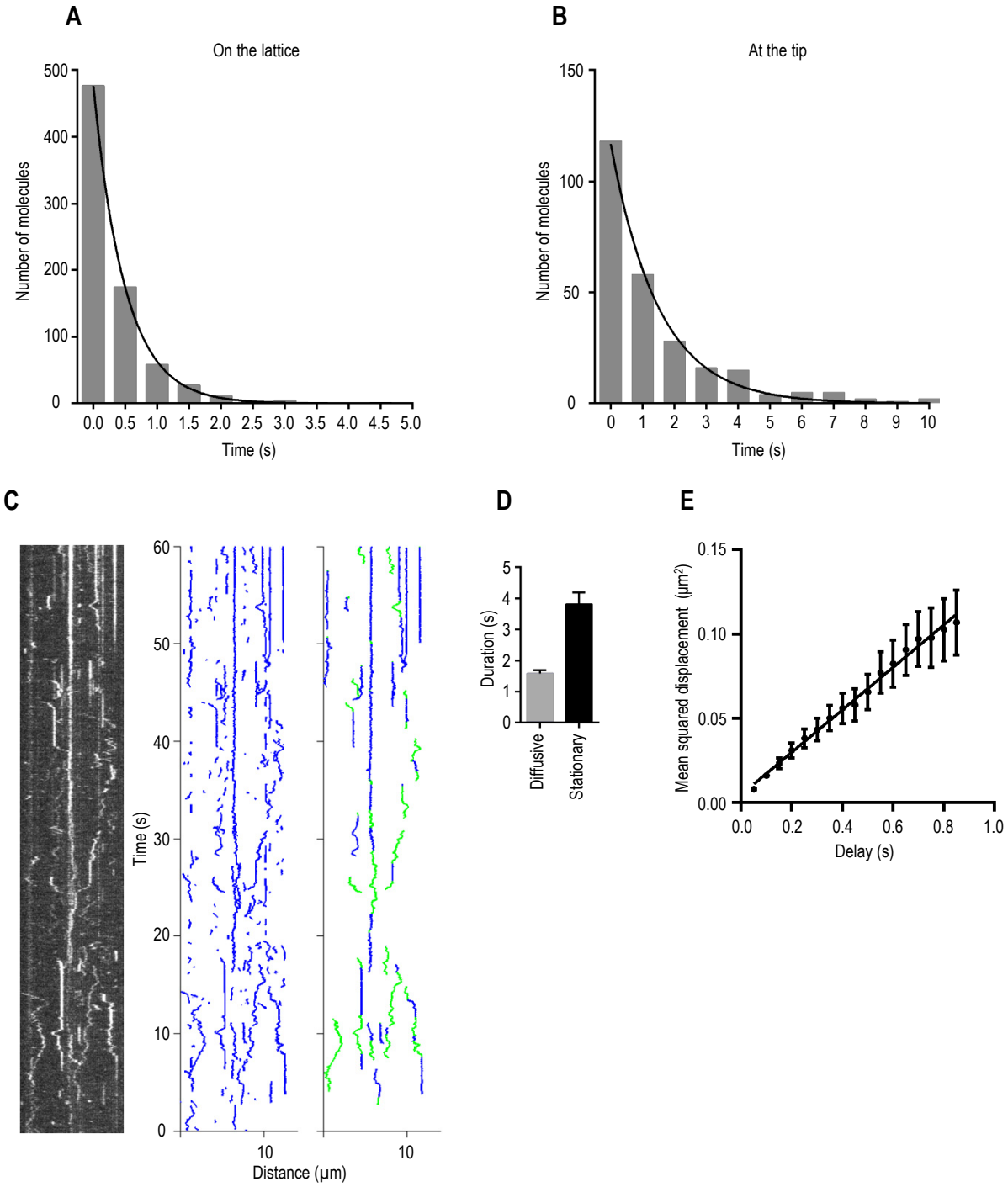
A
On the lattice
Number of molecules
Time (s)
B
At the tip
Number of molecules
Time (s)
C
Time (s)
Distance (μm)
D
Duration (s)
Diffusive
Stationary
E
Mean squared displacement (μm²)
Delay (s)

Figure S3, related to Figure 4. Characterization of $CPAP_{mini}$ single molecule behavior at the tip and on the lattice of dynamic microtubules.

(A-B) Exponential fits of the distributions of dwell times on the microtubule lattice (A) and at the tip (B) for single molecules of $CPAP_{mini}$-GFP.

(C) Representative kymograph illustrating $CPAP_{mini}$-GFP movement on a microtubule (left), corresponding reconstructed tracking results of individual molecules (n=192) (middle), the same tracks filtered for duration (>1.5 s) and color coded depending on the motion behavior: stationary (blue) and diffusive (green) segments (n=29) (right).

(D) Average duration of stationary and diffusive stages of $CPAP_{mini}$-GFP motion (n=134, n=139).

(E) Average mean squared displacement of the diffusive fragments of tracks shown in (C); the line represents linear fit. Error bars represent SEM.

Figure S4

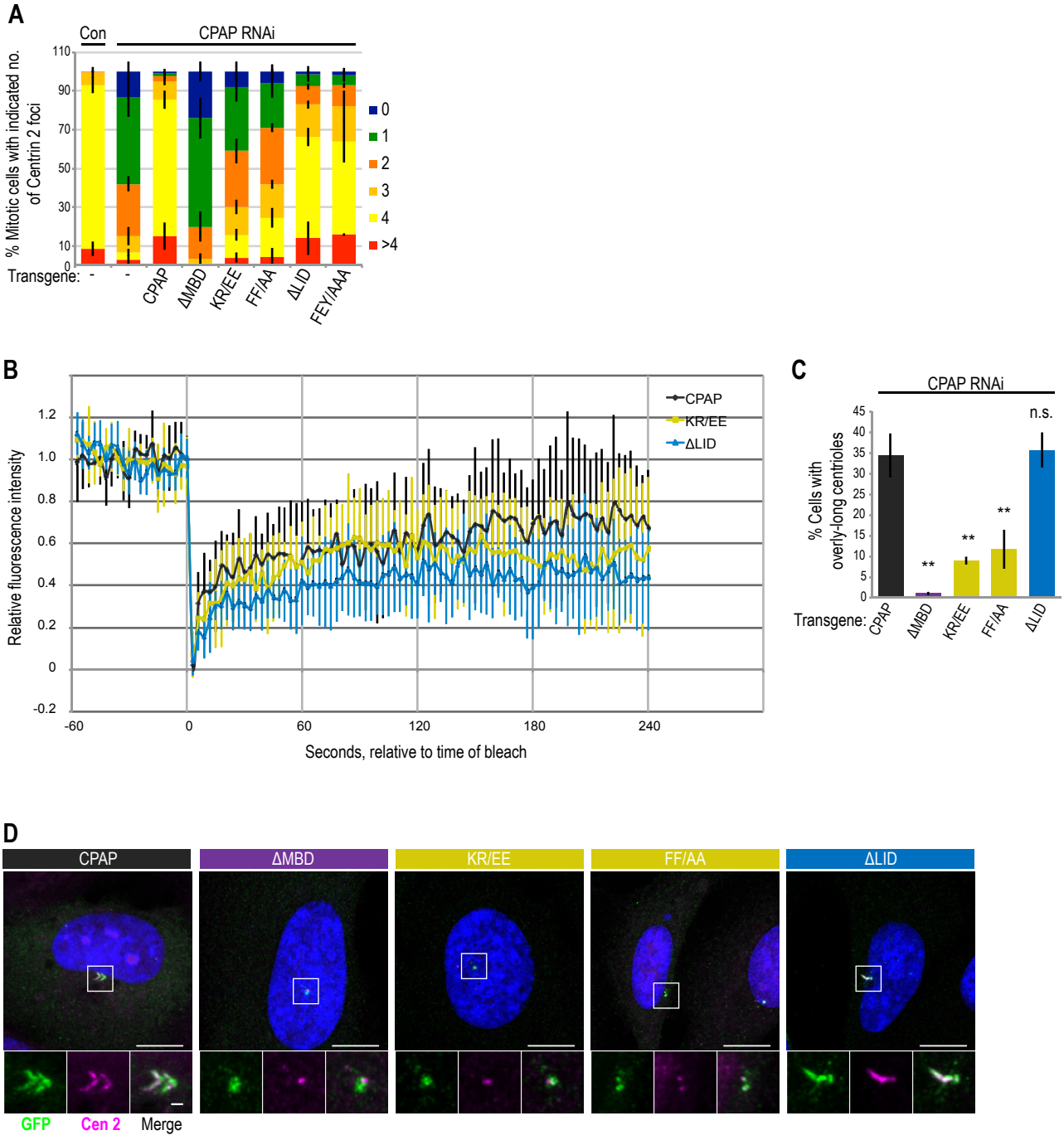
A
Con
CPAP RNAi
% Mitotic cells with indicated no. of Centrin 2 foci
110
90
70
50
30
10
0
0
1
2
3
4
>4
Transgene:
-
-
CPAP
ΔMBD
KR/EE
FF/AA
ΔLID
FEY/AAA
B
Relative fluorescence intensity
1.2
1.0
0.8
0.6
0.4
0.2
0
-0.2
-60
0
60
120
180
240
Seconds, relative to time of bleach
CPAP
KR/EE
ΔLID
C
CPAP RNAi
% Cells with overly-long centrioles
45
40
35
30
25
20
15
10
5
0
n.s.
**
**
**
Transgene:
CPAP
ΔMBD
KR/EE
FF/AA
ΔLID
D
CPAP
ΔMBD
KR/EE
FF/AA
ΔLID
GFP
Cen 2
Merge

Figure S4, related to Figure 5. CPAP SAC domain and MBD, but not the LID domain, are required for centriole over-elongation

(A) Centrin 2 foci scored in mitotic cells expressing the indicated YFP-CPAP variants and depleted of endogenous CPAP by RNAi. Same experiment as shown in Figure 5I, but with all categories displayed. Error bars show the standard deviation of at least 3 experimental replicates, n>100 cells for each sample.

(B) U2OS FlpIn TREX cell lines conditionally expressing indicated YFP-CPAP variants subjected to CPAP RNAi and transgene induction for 72 hours before FRAP analysis. Graph shows mean values, normalized to the mean of the averaged pre-bleach frames for each sample. N = 11 (wild type CPAP and KR/EE), and n = 13 (ΔLID). Time relative to bleach indicated in seconds. Error bars indicate the standard deviation for each time point.

(C, D) U2OS episomal cell lines conditionally expressing indicated GFP-CPAP variants and depleted of endogenous CPAP using RNAi were fixed and stained with anti-GFP and anti-Centrin 2 antibodies 72 hours after RNAi and transgene induction. Scale bar, 10 μm, and 1 μm in insets. Boxes indicate enlarged regions. (C) Proportion of cells with overly long centrioles amongst cells that contain at least one centriole. Note that in all conditions where cells harbored fewer centrioles (see Figure 6A), overly long centrioles were observed less frequently. Average of 3 experimental replicates shown, n >100 cells per experiment. Error bars show standard deviation. Students' paired two-tailed t-test comparing each cell line to the CPAP wild type control: ** indicates $p<0.01$.

Figure S5

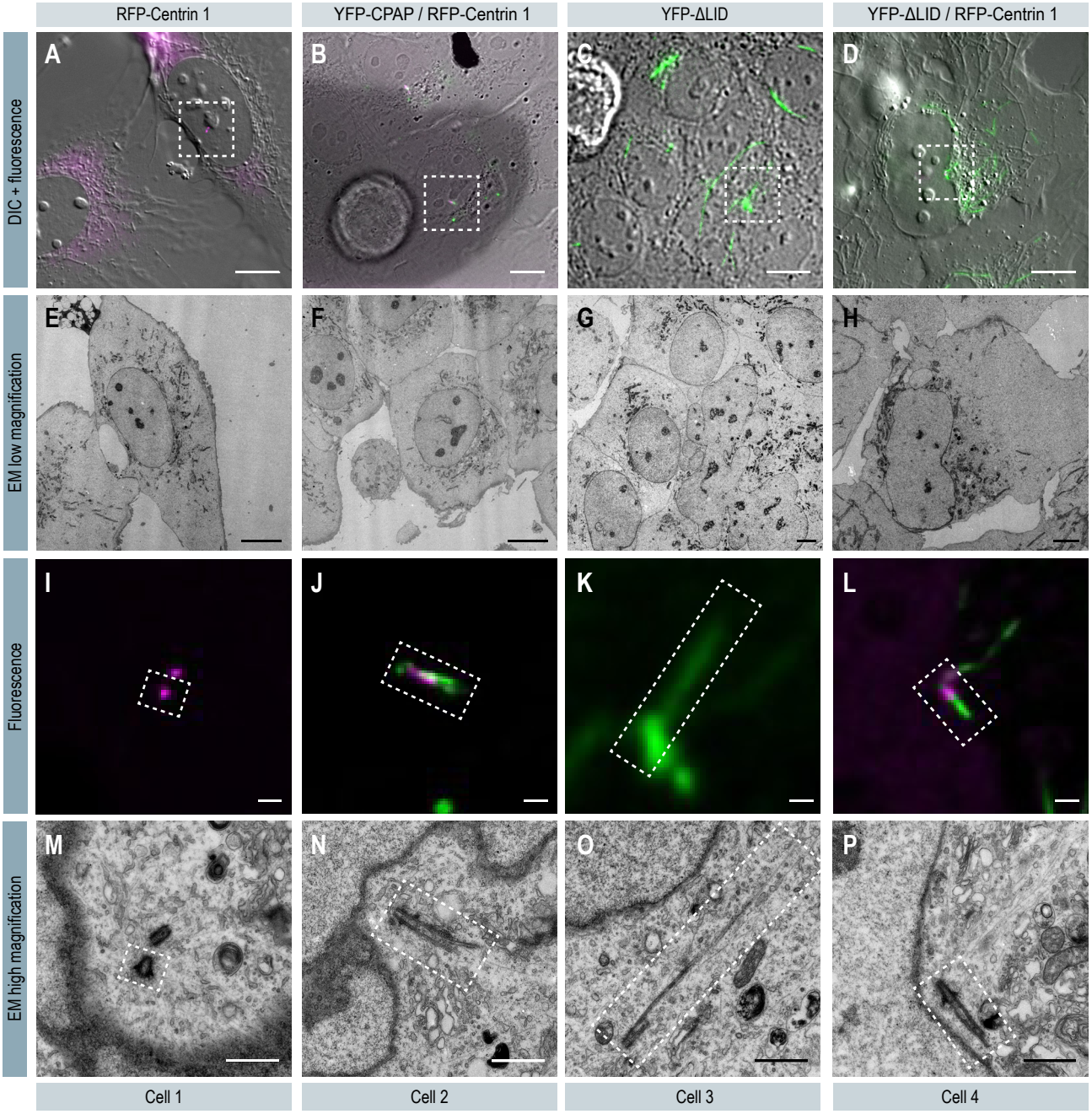
RFP-Centrin 1
YFP-CPAP / RFP-Centrin 1
YFP-ΔLID
YFP-ΔLID / RFP-Centrin 1
DIC + fluorescence
EM low magnification
Fluorescence
EM high magnification
A
B
C
D
E
F
G
H
I
J
K
L
M
N
O
P
Cell 1
Cell 2
Cell 3
Cell 4

Figure S5, related to Figure 7. Correlative light and electron microscopy of cells expressing YFP-CPAP and YFP- ΔLID

(A-D) Differential interference microscopy (DIC) and fluorescence (YFP, RFP, or both) images of the cells shown in Figure 7. Scale bar, 10 μm. Boxes indicate regions shown in I-P.

(E-H) Corresponding low magnification electron microscopy (EM) images of the above cells of interest. Scale bars, 10 μm.

(I-L) High magnification fluorescence images of the regions of interest indicated in (A, E, I, M). Scale bar, 1 μm. Boxes indicate regions shown in Figure 7.

(M-P) High magnification EM images of the regions shown in (C, G, K, O). Scale bars, 1 μm. Boxes indicate regions shown in Figure 7.

Figure S6

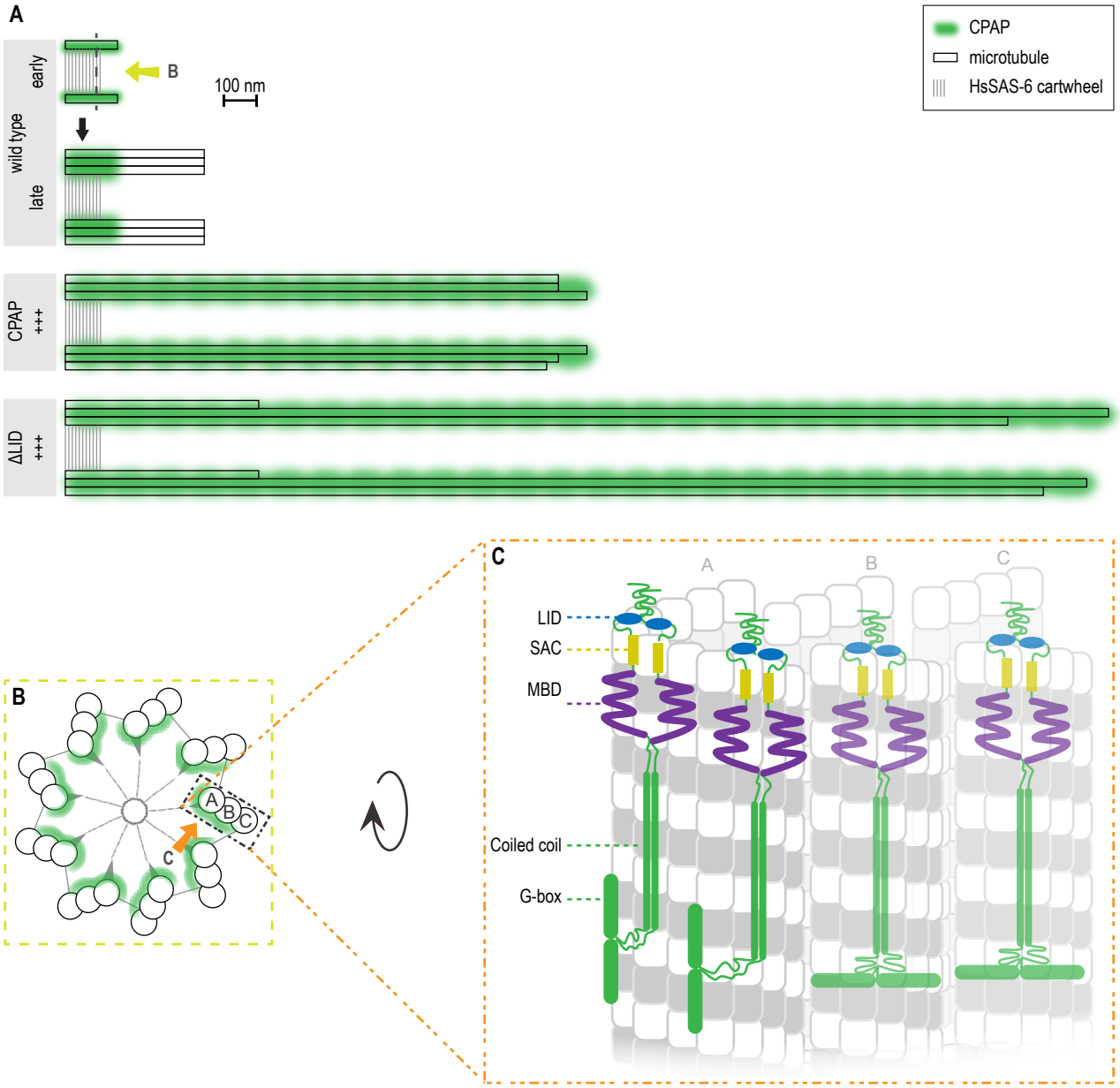
A
wild type
early
late
B
100 nm
CPAP
microtubule
HsSAS-6 cartwheel
CPAP +++
ΔLID +++
B
A
B
C
C
A
B
C
LID
SAC
MBD
Coiled coil
G-box

Figure S6, related to Figure 7. Working model of CPAP's mechanism of action in the context of centrioles.

(A) CPAP (green) is recruited after the assembly of the HsSAS-6-containing cartwheel (gray lines) and the first microtubule (black rectangle). At these early stages of procentriole formation, CPAP is located in the region of the cartwheel and extends slightly more distally. It is during these early stages that CPAP is expected to normally exert its regulation of centriolar microtubule growth. At later stages, CPAP remains in the proximal region of the wild type centriole. Upon overexpression of CPAP (CPAP +++), excess protein localizes along the full length of the centriole, causing over-elongation of centriolar microtubules and the entire distal centriole structure that contains Centrins 1 and 2, and POC5. Overexpression of CPAP-ΔLID (ΔLID +++) results in abnormally elongated centriolar microtubules, which are longer, on average, than the overly-long centrioles observed upon CPAP overexpression, more variable in length, and also lack distal centriole markers such as Centrin and POC5. We refer to these structures as centriole fibers. Light green arrow indicates the direction of view for panel B.

(B) Schematic of a cross section of the centriole looking at the cartwheel-containing region from the distal end. A, B, and C indicate one triplet microtubules. Green indicates the expected position of CPAP, and the orange arrow the direction of view for panel C.

(C) View of the inside surface of a centriolar microtubule triplets with a schematic representation of the position of CPAP dimers (green). CPAP domains are labeled. CPAP dimers located at the tip of the microtubules have their LID domains bound at the end of the β-tubulin subunit, therefore restricting binding of new tubulin dimers to the growing microtubule plus end. CPAP dimers located further down the lattice no longer have their LID domains engaged with tubulin dimers, as the binding interface is occluded, but the SAC and MBD regions still interact with microtubules (not shown). Note that the G-box of the CPAP dimers located on the left are facing inwards the centriole to denote its known interaction with STIL. Note also that whether CPAP is present on all three microtubules in the triplet, and, if so, in how many copies, is not known at present.

Table S1, related to Figures 1, 2, 3 and 5. Constructs used in this study.

Constructs used for structural and biophysical studies	
PN2-3	HsCPAP 311-422
PN2-3s	HsCPAP 319-394
FF/AA	PN2-3 F375A F385A
KR/EE	PN2-3 K377E R378E
FEY/AAA	PN2-3 F338A E399A Y341A
LIDp	PN2-3 311-372
SACp	PN2-3 370-386
Constructs used for in vitro reconstitution studies	
$CPAP_{mini}$	HsCPAP 311-607 GCN4-TEV-eGFP
$CPAP_{mini}$ ΔPN2-3	$CPAP_{mini}$ D311-421
$CPAP_{mini}$ ΔLID	$CPAP_{mini}$ D311-369
$CPAP_{mini}$ FF/AA	$CPAP_{mini}$ F375A F385A
$CPAP_{mini}$ KR/EE	$CPAP_{mini}$ K377E R378E
$CPAP_{mini}$ FEY/AAA	$CPAP_{mini}$ F338A E399A Y341A
$CPAP_{mini}$ ΔMBD	$CPAP_{mini}$ D423-607
$CPAP_{long}$	HsCPAP 312-1053 eGFP
Constructs used for in cellulo studies	
CPAP	HsCPAP
CPAP ΔLID	CPAP D337-350
CPAP FF/AA	CPAP F375A F385A
CPAP KR/EE	CPAP K377E R378E
CPAP ΔMBD	CPAP D423-607

Table S2, related to Figure 1. X-Ray Data Collection and Refinement Statistics.

Data Collection[a]	
Wavelength, Å	1
Space group	P 1 21 1
Resolution range, Å[b]	51.2 - 2.2 (2.28 - 2.2)
Unit cell a, b, c (Å) a, b, g (°)	61.08 85.34 98.69 90 91.77 90
No. of observed reflections	343192 (34254)
No. of unique reflections	51516 (5113)
Mean I/sigma(I)	18.11 (3.19)
R-merge	0.07782 (0.7067)
R-meas	0.09149
$CC_{1/2}$[c]	0.999 (0.87)
CC*	1 (0.964)
Refinement	
R-work	0.1744 (0.2656)
R-free	0.2197 (0.3144)
Number of Macromolecules	7716
Number of Ligands	90
Number of Waters	476
Number of Protein residues	990
RMS(bonds) (Å)	0.021
RMS(angles) (°)	1.03
Ramachandran favored (%)[d]	98
Ramachandran outliers (%)[d]	0.1
B-factors	
Average B-factor	46.57
Macromolecules	46.94
Ligands	35.26
Solvent	42.77

[a] Highest resolution shell statistics are in parentheses.
[b] Resolution cutoffs were chosen based on $CC_{1/2}$ and Mean I/sigma(I) (Karplus and Diederichs, 2012)
[c] As defined by Karplus and Diederichs (Karplus and Diederichs, 2012)
[d] As defined by MolProbity (Davis et al., 2004)

Table S3, related to Figure 4. Characteristics of $CPAP_{mini}$-GFP motion.

Parameter	Mean ± SEM
Average duration of stationary fragment (s)	1.58 ± 0.01
Average duration of diffusive motion (s)	3.81 ± 0.38
Fraction of time spent in diffusive motion (%)	19.7
Diffusion coefficient ($\mu m^2/s$)	0.0257 ± 0.0004
Total number of tracks before filtering	5130
Total number of tracks after filtering	550
Total number of kymographs analyzed	37

Supplemental Experimental Procedures

Protein and peptide preparation

The PN2-3 domain of human CPAP (residues 311-422) and its shorter variant PN2-3s (residues 319-394) were PCR amplified form a *Hs*CPAP clone (Kitagawa et al., 2011) and inserted into the PSTCm1 vector (Olieric et al., 2010) with a N-terminal 6xHis-tag. The DARPin D1 (Pecqueur et al., 2012) was synthesized (GENEWIZ Inc.) and cloned in a T7 pET-based expression vector (Kammerer et al., 1998) with a N-terminal 6xHis-tag. The various CPAP constructs and mutants used in the study are described in Table S1. All PN2-3 mutants were obtained by PCR based mutagenesis. All clones were sequence verified.

Standard protein expression was carried out in the *E. coli* strain BL21(DE3) by induction with 1 mM IPTG at 20 °C. Cells were lysed in a lysis buffer containing 50 mM Tris-HCl, pH 7.5, supplemented with 500 mM NaCl, 10% Glycerol, 10 mM imidazole, 1 mM beta-mercaptoethanol and protease inhibitor cocktail (Roche). Proteins were purified by IMAC using HiTrap Ni-NTA columns (GE Healthcare) followed by size exclusion chromatography on a Superdex 16/60 S75 column. SACp was prepared synthetically using standard peptide synthesis methodology.

Crystallization and structure determination

Bovine brain tubulin was purchased from the Centro de Investigaciones Biológicas (Microtubule Stabilizing Agents Group), CSIC, Madrid, Spain. The flexible C-terminal tails of tubulin were cleaved using subtilisin as described previously (Knipling et al., 1999). Briefly, tubulin was buffer exchanged using a PD-10 desalting column (GE Healthcare) to a buffer containing 10 mM MES pH 6.9, 0.1 mM $MgCl_2$, 0.1 mM EGTA and 1mM of GTP. Subtilisin (Sigma Cat. no. P8038) was added in a weight ratio of 1:100 to a tubulin solution (3 mg/ml) and incubated for 45 minutes at 25 °C. Cleavage was stopped by adding 1 mM PMSF. The reaction mixture was further incubated on ice for 30 minutes followed by centrifugation for 30 minutes at 300,000 x g using an MLA-130 rotor (Beckman Coulter). The supernatant was collected and cleavage efficiency was accessed by a Coomassie stained 7.5% SDS PAGE (Banerjee et al., 2010). The cleaved tubulin was buffer-exchanged to BRB80 (PIPES-KOH, pH 6.8, supplemented with 80 mM, 1 mM $MgCl_2$, 1 mM EGTA) using a PD-10 desalting column (GE Healthcare).

Equimolar amounts of D1, PN2-3 and subtilisin-treated tubulin were mixed and the PN2-3-tubulin-D1 complex was concentrated to ~20 mg/ml using a Centriprep device (Mw cutoff 5 kDa; Amicon). PN2-3-tubulin-D1 samples were complemented with 0.2 mM GDP, 1 mM Colchicine and 5 mM DTT before setting up sitting drop vapor diffusion crystallization trials. Crystals were obtained in a condition containing 20% PEG 550 mono methyl ether (MME) and 0.1 M MES, pH 6.5. Precipitant solution supplemented with 10% glycerol was used as a cryo-protectant for freezing crystals. X-ray diffraction data were collected at 100K at beamline X06DA at the Swiss Light Source (Paul Scherrer Institut, Villigen, Switzerland), and were then processed and merged with XDS (Kabsch, 2010).

The PN2-3-tubulin-D1 structure was solved by molecular replacement using the αβ-tubulin-D1 complex structure as a search model (PDB ID 4DRX) and the program Phaser provided in the Phenix software suite (McCoy et al., 2007). The models were first refined with rigid body refinement and simulated annealing refinement in Phenix (Adams et al., 2010). In the refined structure, the difference electron density for PN2-3 allowed us to model the specific residues of the SAC box using Coot (Emsley and Cowtan, 2004). The resulting model was refined by iterative cycles of model building in coot and refinement in Phenix. The quality of the structures was assessed with MolProbity (Chen et al., 2010) and figures were prepared using PyMOL (The PyMOL Molecular Graphics System, version 1.4.1; Schrödinger, LLC). Data collection and refinement statistics are given in Table S2.

ITC experiments

For exchanging the nucleotide of tubulin, bovine brain tubulin was buffer exchanged to a buffer containing 80 mM PIPES-KOH, pH 6.8, supplemented with 1mM EDTA using a PD-10 desalting column (GE Healthcare). 2 mM of GDP, GTP or GMPCPP was added to the samples that were incubated on ice for 10 minutes. Excess nucleotide was removed by another step of buffer exchange using a PD-10 desalting column pre-equilibrated with BRB80 buffer supplemented with 0.5 mM TCEP. PN2-3 variants were buffer exchanged to BRB80 buffer supplemented with 0.5 mM TCEP by overnight dialysis at 4°C.

Standard ITC experiments were performed at 25 °C using an ITC200 system (Microcal). 0.1–0.4 mM PN2-3 variants in the syringe were injected step-wise into a 10-20 μM tubulin solution in the cell. Experiments with tubulin-D1 in the presence of Eribulin (Eisai Co., Ltd) and Maytansine (National Institutes of Health, Open

Chemical Repository Collection) were obtained by incubating equimolar amounts of tubulin and ligand at 4 °C for 15 minutes before setting up the ITC experiment. The resulting heats were integrated and fitted in Origin (OriginLab) using the standard 'one set of sites' model provided by the software package.

Protein purification for in vitro reconstitution assays

$CPAP_{long}$–GFP and $CPAP_{mini}$-GFP variants used in the *in vitro* reconstitutions assays (Table S1) were purified from HEK293T cells using the Strep(II)-streptactin affinity purification. Cells were harvested 2 days post transfection. Cells from a 25 cm dish were lysed in 500 µl of lysis buffer (50 mM HEPES, 300 mM NaCl and 0.5% Triton X-100, pH 7.4) supplemented with protease inhibitors (Roche) on ice for 10 minutes. The supernatant obtained from the cell lysate after centrifugation at 16,000 x g for 20 minutes was incubated with 40 µl of StrepTactin Sepharose beads (GE) for 1 hour. The beads were washed 3 times in the lysis buffer without the protease inhibitors. The protein was eluted with 40 µl of elution buffer (50 mM HEPES, 150 mM NaCl, 1 mM $MgCl_2$, 1 mM EGTA, 1 mM dithiothreitol (DTT), 2.5 mM d-Desthiobiotin and 0.05% Triton X-100, pH 7.4). Purified proteins were snap-frozen and stored at -80 °C. Bacterially expressed mCherry-EB3 was produced as described previously (Montenegro Gouveia et al., 2010) and mCherry-CAMSAP3 was produced in HEK293T cells as described previously (Jiang et al., 2014).

In vitro reconstitution assay

Reconstitution of microtubule growth dynamics *in vitro* was performed as described previously (Montenegro Gouveia et al., 2010). GMPCPP microtubule seeds (70% unlabeled tubulin, 18% biotin tubulin and 12% rhodamine tubulin) were prepared as described before (Gell et al., 2010). Flow chambers, assembled from plasma-cleaned glass coverslips and microscopic slides were functionalized by sequential incubation with 0.2 mg/ml PLL-PEG-biotin (Susos AG, Switzerland) and 1 mg/ml NeutrAvidin (Invitrogen) in MRB80 buffer (80 mM piperazine-*N*,*N*[prime]-bis(2-ethanesulfonic acid), pH 6.8, supplemented with 4 mM $MgCl_2$, and 1 mM EGTA. The microtubule seeds were attached to coverslips through biotin-NeutrAvidin interactions. Flow chambers were further blocked with 1 mg/ml κ-casein. The reaction mix with or without $CPAP_{mini}$ proteins (MRB80 buffer supplemented with 15 µM porcine brain tubulin, 0.5 µM rhodamine-tubulin, 50 mM KCl, 1 mM guanosine triphosphate, 0.2 mg/ml κ-casein, 0.1% methylcellulose, and oxygen scavenger mix [50 mM glucose, 400 µg/ ml glucose oxidase, 200 µg/ml catalase, and 4 mM DTT]) was added to the flow chamber after centrifugation in an Airfuge for 5 minutes at 119,000 × *g*. For experiments in the presence of EB3, concentration of mCherry-EB3 was 20 nM and rhodamine-tubulin was excluded from the assay. Rhodamine-tubulin was also excluded from the assay with $CPAP_{mini}$-GFP and mCherry-CAMSAP3. The flow chamber was sealed with vacuum grease, and dynamic microtubules were imaged immediately at 30 °C using Total Internal Reflection Fluorescence (TIRF) microscopy. All tubulin products were from Cytoskeleton Inc.

TIRF microscopy

The in vitro reconstitutions assays were imaged on a TIRF microscope setup as described in (Mohan et al., 2013) or on an $iLas^2$ TIRF setup. In brief, we used an inverted research microscope Nikon Eclipse Ti-E with the perfect focus system, equipped with Nikon CFI Apo TIRF 100x 1.49 N.A. oil objective and controlled with MetaMorph 7.7.5 software (Molecular Devices). The microscope was equipped with TIRF-E motorized TIRF illuminator modified by Roper Scientific France/PICT-IBiSA, Institut Curie. To keep the in vitro samples at 30 °C, a stage top incubator model INUBG2E-ZILCS (Tokai Hit) was used. For excitation, 491 nm 100 mW Calypso (Cobolt) and 561 nm 100 mW Jive (Cobolt) lasers were used. We used ET-GFP 49002 filter set (Chroma) for imaging of proteins tagged with GFP or ET-mCherry 49008 filter set (Chroma) for imaging of proteins tagged with mCherry. Fluorescence was detected using an EMCCD Evolve 512 camera (Roper Scientific) with the intermediate lens 2.5X (Nikon C mount adapter 2.5X) or using the CoolSNAP HQ2 CCD camera (Roper Scientific) without an additional lens. In both cases the final magnification was 0.063 µm/pixel.

$ILas^2$ system (Roper Scientific, Evry, France) is a dual laser illuminator for azimuthal spinning TIRF illumination and with a custom modification for targeted photomanipulation. This system was installed on the Nikon Ti-E microscope with the perfect focus system, equipped with 150 mW 488 nm laser and 100 mW 561 nm laser, 49002 and 49008 Chroma filter sets, EMCCD Evolve mono FW DELTA 512x512 camera (Roper Scientific) with the intermediate lens 2.5X (Nikon C mount adapter 2.5X), CCD camera CoolSNAP MYO M-USB-14-AC (Roper Scientific) and controlled with MetaMorph 7.8.8 software (Molecular Device). To keep the in vitro samples at 30°C, a stage top incubator model INUBG2E-ZILCS (Tokai Hit) was used. The final resolution using Evolve EMCCD camera was 0.065 □m/pixel, using CoolSNAP Myo CCD camera it was 0.045 µm/pixel.

Analysis of microtubule plus end dynamics in vitro

Kymographs were generated using the ImageJ plugin KymoResliceWide (http://fiji.sc/KymoResliceWide). Microtubule dynamics parameters were determined from kymographs using an optimized version of the custom made JAVA plug in for ImageJ as described previously (Jiang et al., 2014; Montenegro Gouveia et al., 2010; Taylor, 1997). ~100-200 microtubule growth events were analyzed per condition.

Intensity analysis for CPAP$_{mini}$ along microtubules

Intensity profiles extraction and alignment of rhodamine-tubulin and CPAP$_{mini}$ were performed using a custom written Matlab routine. First, we obtained the average intensity of microtubule profile along a 4-pixel wide line using the rhodamine-tubulin channel. The same line was used to obtain an intensity profile in the CPAP$_{mini}$ (GFP) channel. After background subtraction, each intensity profile $I(x)$ was normalized:

$$I_{norm}(x) = \frac{I(x) - I_{\min}}{I_{\max} - I_{\min}} \cdot 100\% \quad \mathrm{I_{normalized}} = \left(\frac{\mathrm{I\text{-}I_{min}}}{\mathrm{I_{max}\text{-}I_{min}}}\right) \mathrm{xd}$$

with respect to the maximum and minimum intensity values along the whole profile. The normalized intensity profiles of different microtubules were aligned so that the plus end tip position was at the origin of the coordinates (Figure 3C). The plus end position was determined by fitting the rhodamine-tubulin profile to a Gaussian survival function using equation:

$$I_{norm}(x) = \frac{1}{2} I_{MT} erfc\left(\frac{x - x_{PF}}{\sqrt{2}\sigma_{PF+PSF}}\right) + I_{BG}$$

where erfc is the complimentary error function, I_{MT} and I_{BG} are average intensities of the microtubule and the background, x_{PF} is the position of plus end tip and σ_{PF+PSF} is the standard deviation of the microtubule tip taper combined with the one for the microscope point spread function.

Single-molecule fluorescence intensity analysis of CPAP$_{mini}$

Sample preparation for the fluorescence intensity analysis was performed by immobilizing diluted GFP or CPAP$_{mini}$-GFP proteins non-specifically to the plasma cleaned glass coverslips in flow chambers. After protein addition the flow chambers were washed with MRB80 buffer, sealed with vacuum grease and immediately imaged with a TIRF microscope. 10-20 images of previously unexposed coverslip areas were acquired with 100 ms exposure time and low laser power. GFP and CPAP$_{mini}$-GFP were located in different chambers of the same coverslip, so the same imaging conditions could be preserved. Single molecule fluorescence spots were detected and fitted with 2D Gaussian function using custom written ImageJ plugin DoM_Utrecht (https://github.com/ekatrukha/DoM_Utrecht). The fitted peak intensity values were used to build fluorescence intensity histograms.

Single molecule diffusion and kinetics analysis

The study of single molecule kinetics of CPAP$_{mini}$ at the tip and lattice of dynamic microtubules was performed in the presence of 100 nM CPAP$_{mini}$-mCherry, 5 nM CPAP$_{mini}$-GFP and rhodamine tubulin. Kymographs were generated for each microtubule over 60 seconds with 50 millisecond intervals. The residence times at the microtubule tip and lattice were manually obtained from kymographs. Histograms of times for both conditions were fitted to a single exponential decay function in GraphPad Prism 6. The reported mean residence time at the lattice and tip were obtained from these fits. The mean residence time was corrected for photo bleaching as described (Helenius et al., 2006). The characteristic time constant of photobleaching was estimated by fitting the total field of view intensity of CPAP$_{mini}$ movies over time to a single exponential decay function. The value of averaged photobleaching time constant over 15 movies was used for correction.

Coordinates of individual fluorescent spots of CPAP$_{mini}$-GFP diffusing along microtubule were derived from the detection performed using the ImageJ plugin DOM_Utrecht as described above. Detections were linked to 2D tracks using nearest neighbor linking algorithm of the same plugin with a search radius of 0.5-1 μm. Coordinates

of all time points of all the tracks along the same microtubule were fitted to a straight line and subsequently projected on it resulting in 1D tracks. Only tracks longer than 1.5 seconds were considered. Mean squared displacement (MSD) analysis was performed using msdanalyzer Matlab routine (Tarantino et al., 2014). To separate the periods of stationary and diffusive motion for each track MSD (τ) was calculated by internal averaging for a sliding window of 30 frames. The first 7 point (excluding zero) were used to fit $MSD(\tau)=0.5D\tau+b$, with D termed the 1D diffusion coefficient and b as a localization precision error. For each fit we calculated the coefficient of determination R^2 characterizing the quality of fit. Track fragments where R^2 was above the threshold of 0.7 were considered as "diffusing state", since the sliding window MSD fitted well with linear dependence (green tracks in Figure S3C, right panel). The rest of the track was considered being in the "stationary state" (blue fragments in Figure S3C, right panel). The diffusion coefficient reported in Supplementary Table S3 was calculated by averaging all D values from all fits where $R^2>0.7$ (n=8959).

$CPAP_{mini}$ molecule counting at microtubule tips

To determine the number of molecules of $CPAP_{mini}$ at a microtubule tip, we immobilized single molecules of $CPAP_{mini}$ onto the coverslip of one of the flow chambers and performed the *in vitro* reconstitution assay in the adjacent chamber of the same coverslip. Images of unbleached $CPAP_{mini}$ single molecules were acquired first and using the same imaging/illumination conditions, time lapse imaging was performed on the *in vitro* assay with $CPAP_{mini}$, using 100 ms exposure and 2 second intervals for 5 minutes. The plus end localized $CPAP_{mini}$ molecules were manually located in each frame and fitted with 2D Gaussian, the amplitude of which was used for the intensity analysis. To build the distributions of $CPAP_{mini}$ molecule numbers at the microtubule tip, each $CPAP_{mini}$ intensity value at the microtubule plus end was normalized by the average $CPAP_{mini}$ single molecule intensity from the adjacent chamber.

Statistical Analysis

The relative standard error for catastrophe frequency was calculated as described (Taylor, 1997). The relative standard error of mean rescue frequency in the experiments with $CPAP_{mini}$ constructs was calculated in the same way as the standard error of the mean catastrophe frequency, i.e. $SE_r = \bar{f}_r \frac{SE_{t_{sh}}}{\bar{t}_{sh}}$, where $\bar{f}_r, \bar{t}_{sh}$ are average values and $SE_{f_r}, SE_{t_{sh}}$ are standard errors of rescue frequency and shortening time respectively. The number of observed rescue events for control was relatively small as compared to the catastrophes, so we assumed that they follow a Poisson distribution. The standard deviation of the rescue frequency was calculated as the square root of its mean value and the standard error was calculated according to $SE_{f_r} = \frac{\sqrt{\bar{f}_r}}{\sqrt{N_r}}$, where $\bar{f}_r$ and SE_{f_r} are the average and the standard error of the rescue frequency and N_r is the number of rescues (Smal et al., 2009).

Generation of expression vectors for cell biology

A cDNA encoding siRNA resistant CPAP was cloned into pENTR 1A, as previously described (Kitagawa et al., 2011). This vector was used for site directed mutagenesis reactions to produce KR/EE and FF/AA mutations using Quikchange Site Directed Mutagenesis kit (Agilent). Deletions ΔLID and ΔMBD were generated using Phusion polymerase (NEB). For deletion mutants, linear PCR products were generated with 10 bp overlapping regions and ligated using CloneEZ (GenScript). Entry vectors were then used in LR Clonase reactions (Invitrogen) with pEBTet-EGFP-GW (Kitagawa et al., 2011) or pcDNA5FRT/TO-YFP-GW (gift from Zuzana Hořejší) to produce expression vectors. All Entry clones were sequence-verified.

Cell culture, transfections, cell line generation, and siRNAs

U2OS cells were cultured in high-glucose DMEM with GlutaMAX (Invitrogen) supplemented with 10% fetal calf serum (FCS) in a humidified 5% CO_2 incubator at 37 °C. To generate inducible cell lines with the pEBTet-EGFP vector, cells were transfected with the appropriate vectors using Lipofectamine 2000 (Invitrogen) and selected using 1 μg/ml puromycin 24 hours after transfection, as previously described (Kitagawa et al., 2011). For generating stable integrated cell lines, we used a U2OS FlpIn TREX cell line, a gift from Erich Nigg (Arquint and Nigg, 2014). U2OS FlpIn TREX cells were transfected using Lipofectamine 2000 with a 3:1 ratio

of pcDNA5-FRT/TO-YFP-CPAP vectors:pOG44 (Invitrogen Flp-In System). Cells were selected using 100 µg/ml Hygromycin B and 10 µg/ml Blasticidin (both from InvivoGen) for 1-2 weeks, until all untransfected cells were dead. For both types of cell line, 1 µg/ml doxycycline was used to induce transgene expression (Sigma-Aldrich). CPAP RNAi was carried out at 60 nM as previously described (Kitagawa et al., 2011) and Stealth siRNA Negative Control Lo GC was used as a negative control, also at 60 nM. Unless otherwise indicated, RNAi was carried out for 72 hour before fixation of the cells, with simultaneous induction of transgene expression with 1 µg/ml Doxycycline. Note that cells expressing KR/EE often exhibited large globular YFP aggregates, but never microtubule decoration, perhaps explaining the absence of centrosomal fibers in this mutant compared to FF/AA (see Figure 6A).

Correlative light and electron microscopy (CLEM)

Cells were cultured on glass coverslips coated on one side with a 3 nm thick layer of carbon, with an additional layer of 10 nm thickness to reveal a gridded pattern with a coordinate system of letters for locating the cell of interest by light microscopy, and also once the cells were resin embedded. Endogenous CPAP was depleted by RNAi for 72 hours, simultaneous with induction of the transgene. For dual marker experiments, cells were transfected with a tagRFP-Centrin 1 expression vector 16 hours prior to fixation (Keller et al., 2014). Cells were fixed in a solution of 0.1 % glutaraldehyde and 2.0 % paraformaldehyde in 0.1 M phosphate buffer, pH 7.4, for 2 hours, then washed thoroughly with cacodylate buffer (0.1 M, pH 7.4), and imaged by wide field light microscopy using a Zeiss Plan-Apochromat 63 x oil-immersion objective, NA 1.40. Z-sections were imaged at an interval of ~0.3 µm. Fluorescence images shown in Figure 7 are single plane images deconvolved using Huygens Core 15.10 software (Scientific Volume Imaging, SVI) through the web interface Huygens Remote Manager. A theoretical Point Spread Function (PSF) was used in combination with the "Classic Maximum Likelihood Estimation" algorithm, an automatic background estimation and stopping criteria of 40 iterations and 0.1 quality change. The deconvolution settings and signal to noise ratios were set according to SVI's recommendations. Immediately after imaging, samples were post-fixed for 40 minutes in 1.0 % osmium tetroxide, then 30 minutes in 1.0% uranyl acetate in water, before being dehydrated through increasing concentrations of alcohol and then embedded in Durcupan ACM resin (Fluka, Switzerland). The coverslips were then placed face down on a glass slide coated with mold releasing agent (Glorex, Switzerland), with approximately 1 mm of resin separating the two. The resin was initially hardened for 12 hours in a 65 °C oven and then the coverslips detached from the resin by immersing them alternately into hot (60 °C) water followed by liquid nitrogen. The smooth resin surface, with the cells embedded, also showed the grid pattern, which was used to locate the region of interest imaged by light microscopy. These regions were mounted on blank resin blocks with acrylic glue and trimmed with glass knives to form a block ready for serial sectioning. Series of between 150 and 300 thin sections (50 nm thickness) were cut with a diamond knife mounted on an ultramicrotome (Leica UC7), and collected onto single-slot, copper grids with a pioloform support film. These sections were contrasted with lead citrate and uranyl acetate, and images taken using an FEI Spirit TEM with Eagle CCD camera. Images of each cell of interest were taken on every section in which it appeared and these images aligned using Photoshop (Adobe). The aligned series was then matched with the light microscopy images to correlate the position of the fluorescent signal with the underlying ultrastructure.

Fluorescence Recovery After Photo-bleaching (FRAP)

Cells were grown in glass bottomed cell culture dishes (Matek) and imaged in a humidified 5% CO_2 incubator at 37 °C in DMEM high glucose medium without phenol red (GE Healthcare), supplemented with 15% FCS, 20 mM HEPES buffer (Gibco), 1 mM sodium pyruvate (Sigma), and Penicillin/Streptomycin (Gibco). We used a Zeiss LSM 710 with an N-Achromat 63x water immersion objective NA 0.90, controlled with Zeiss Zen software to bleach a circular region of 25 pixel diameter (pixel size 0.14 µm) around the centrosome using 10 iterations with the 514 nm laser at 100%, and acquisition of a 60 x 60 pixel region with a pixel dwell time of 2.77 µsec and 2 x averaging. Cells were imaged every 3 seconds, for one minute pre- and 4 minutes post-bleach. Analysis was carried out using Image J, with a plugin to automatically detect a circular region of interest of 15 pixel diameter using a Gaussian blurring factor of 5 and the brightest pixel to center the region of interest. Before measuring fluorescence intensity, the regions of interest were manually curated to ensure that the centrosome was contained within it. All FRAP curves were normalized to the average of the first 20 pre-bleach intensities.

Supplemental References

Adams, P.D.et al. (2010). PHENIX: a comprehensive Python-based system for macromolecular structure solution. Acta Crystallogr. D. Biol. Crystallogr. *66*, 213-221.

Arquint, C. and Nigg, E.A. (2014). STIL microcephaly mutations interfere with APC/C-mediated degradation and cause centriole amplification. Curr. Biol. *24*, 351-360.

Azimzadeh, J., Hergert, P., Delouvee, A., Euteneuer, U., Formstecher, E., Khodjakov, A., and Bornens, M. (2009). hPOC5 is a centrin-binding protein required for assembly of full-length centrioles. J. Cell Biol. *185*, 101-114.

Banerjee, A., Bovenzi, F.A., and Bane, S.L. (2010). High-resolution separation of tubulin monomers on polyacrylamide minigels. Anal. Biochem. *402*, 194-196.

Chen, V.B., Arendall, W.B., III, Headd, J.J., Keedy, D.A., Immormino, R.M., Kapral, G.J., Murray, L.W., Richardson, J.S., and Richardson, D.C. (2010). MolProbity: all-atom structure validation for macromolecular crystallography. Acta Crystallogr. D. Biol. Crystallogr. *66*, 12-21.

Davis, I.W., Murray, L.W., Richardson, J.S., and Richardson, D.C. (2004). MOLPROBITY: structure validation and all-atom contact analysis for nucleic acids and their complexes. Nucleic Acids Res. *32*, W615-W619.

Emsley, P. and Cowtan, K. (2004). Coot: model-building tools for molecular graphics. Acta Crystallogr. D. Biol. Crystallogr. *60*, 2126-2132.

Gell, C.et al. (2010). Microtubule dynamics reconstituted in vitro and imaged by single-molecule fluorescence microscopy. Methods Cell Biol. *95*, 221-245.

Helenius, J., Brouhard, G., Kalaidzidis, Y., Diez, S., and Howard, J. (2006). The depolymerizing kinesin MCAK uses lattice diffusion to rapidly target microtubule ends. Nature *441*, 115-119.

Jiang, K.et al. (2014). Microtubule minus-end stabilization by polymerization-driven CAMSAP deposition. Dev. Cell *28*, 295-309.

Kabsch, W. (2010). XDS. Acta Crystallogr. D. Biol. Crystallogr. *66*, 125-132.

Kammerer, R.A., Schulthess, T., Landwehr, R., Lustig, A., Fischer, D., and Engel, J. (1998). Tenascin-C hexabrachion assembly is a sequential two-step process initiated by coiled-coil alpha-helices. J. Biol. Chem. *273*, 10602-10608.

Karplus, P.A. and Diederichs, K. (2012). Linking crystallographic model and data quality. Science *336*, 1030-1033.

Kitagawa, D., Kohlmaier, G., Keller, D., Strnad, P., Balestra, F.R., Fluckiger, I., and Gönczy, P. (2011). Spindle positioning in human cells relies on proper centriole formation and on the microcephaly proteins CPAP and STIL. J. Cell Sci. *124*, 3884-3893.

Knipling, L., Hwang, J., and Wolff, J. (1999). Preparation and properties of pure tubulin S. Cell Motil. Cytoskeleton *43*, 63-71.

McCoy, A.J., Grosse-Kunstleve, R.W., Adams, P.D., Winn, M.D., Storoni, L.C., and Read, R.J. (2007). Phaser crystallographic software. J Appl Crystallogr. *40*, 658-674.

Mohan, R., Katrukha, E.A., Doodhi, H., Smal, I., Meijering, E., Kapitein, L.C., Steinmetz, M.O., and Akhmanova, A. (2013). End-binding proteins sensitize microtubules to the action of microtubule-targeting agents. Proc. Natl. Acad. Sci. U. S. A *110*, 8900-8905.

Montenegro Gouveia, S.et al. (2010). In vitro reconstitution of the functional interplay between MCAK and EB3 at microtubule plus ends. Curr. Biol. *20*, 1717-1722.

Olieric, N., Kuchen, M., Wagen, S., Sauter, M., Crone, S., Edmondson, S., Frey, D., Ostermeier, C., Steinmetz, M.O., and Jaussi, R. (2010). Automated seamless DNA co-transformation cloning with direct expression vectors applying positive or negative insert selection. BMC. Biotechnol. *10*, 56.

Pecqueur, L., Duellberg, C., Dreier, B., Jiang, Q., Wang, C., Pluckthun, A., Surrey, T., Gigant, B., and Knossow, M. (2012). A designed ankyrin repeat protein selected to bind to tubulin caps the microtubule plus end. Proc. Natl. Acad. Sci. U. S. A *109*, 12011-12016.

Schindelin, J.et al. (2012). Fiji: an open-source platform for biological-image analysis. Nat. Methods *9*, 676-682.

Smal, I., Grigoriev, I., Akhmanova, A., Niessen, W.J., and Meijering, E. (2009). Accurate estimation of microtubule dynamics using kymographs and variable-rate particle filters. Conf. Proc. IEEE Eng Med. Biol. Soc. *2009*, 1012-1015.

Tarantino, N., Tinevez, J.Y., Crowell, E.F., Boisson, B., Henriques, R., Mhlanga, M., Agou, F., Israel, A., and Laplantine, E. (2014). TNF and IL-1 exhibit distinct ubiquitin requirements for inducing NEMO-IKK supramolecular structures. J. Cell Biol. *204*, 231-245.

Taylor, J.R. (1997). An Introduction to Error Analysis. University Science Books, Sausalito).